This manuscript has been published online in: Dental Materials available online 10 April 2021, Version of Record 12 June 2021
https://doi.org/10.1016/j.dental.2021.03.007

Title: Melatonin-doped polymeric nanoparticles reinforce and remineralize radicular dentin: morpho-histological, chemical and biomechanical studies.

Authors: Manuel Toledano[a], Fátima S. Aguilera[a], Estrella Osorio[a], Manuel Toledano-Osorio[a*], Germaine Escames[b], Antonio L. Medina-Castillo[c], Raquel Toledano[a], Christopher D Lynch[d], Raquel Osorio[a]

Institution:

[a] University of Granada, Faculty of Dentistry. Colegio Máximo de Cartuja s/n 18071, Granada, Spain.

[b] University of Granada, Faculty of Medicine. Parque Tecnológico de la Salud, Av. de la Investigación, 11, 18016, Granada, Spain.

[c] NanoMyP®, Nanomateriales y Polímeros S.L., Spin-Off company of the University of Granada. Edificio BIC-Granada. Av. Innovación 1. 18016, Armilla, Granada, Spain.

[d] University Dental School & Hospital/Cork University Dental School & Hospital, Cork, Ireland.

***Corresponding author:** Manuel Toledano-Osorio

University of Granada, Faculty of Dentistry

Dental Materials Section

Colegio Máximo de Cartuja s/n

18071 – Granada - Spain.

Tel.: +34-958243789

Fax: +34-958240809

Email: rosorio@ugr.es

Acknowledgements

This work was funded by the Ministry of Economy and Competitiveness and European Regional Development Fund (MAT2017-85999P MINECO/AEI/FEDER/UE).

Declaration of interest: None.

Melatonin-doped polymeric nanoparticles reinforce and remineralize radicular dentin: morpho-histological, chemical and biomechanical studies.

Keywords: remineralization, dentin, sealing, microscopy, degradation, mechanical, chemical, melatonin, collagen.

1. Introduction

The concept of apical periodontitis involves an inflammatory disease that affects the peri-radicular tissues and bacterial presence in dental pulp. It is the most common sequel of untreated tooth decay and usually origins tooth loss. Nevertheless, apical periodontitis poses an important host defense reaction destined to confine root canal bacteria and avoid them from spreading into adjacent oral tissues [1]. The interest for strengthening the radicular dentin after periapical periodontitis, abscesses and pulpitis that may indicate endodontic treatment, has increased in the last years [2]. The structure and treatment of radicular dentin gather several peculiarities [3]. An endodontically-treated tooth is prone to fracture because the tooth structure damage caused by carious infection and pulpitis, preparation of cavity and canal instrumentation [4]. Besides, the composition of dentin is not the same across its anatomy, but it changes from the cervical down to the apical zones in root length [5].

Even when eliminating microorganisms from the root canal system before canal filling is the principal aim of endodontic treatment; sealing and remineralization should also be considered [3,6]. Indicated materials as endodontic sealers have ranged from the employ of silicate aluminum based cements [7], glass-ionomer [8], to epoxy resins for radicular canal sealers such as AH-Plus [9], but most of them have presented different clinical limitations [4]. Non-resorbable polymeric NPs doped with antimicrobials and reinforcing agents have successfully been tested in advance [10], but combined anti-inflammatory therapy has not been considered yet. The role of melatonin (ML) in hard tissues has

attracted attention [11]. ML (N-acetyl-5-metoxy-tryptamine) is an indoleamine that is synthesized and secreted by the pineal gland in a circandian pattern [12]. Melatonin is also formed in perhaps all organs in quantities by orders of magnitude higher than in the pineal gland and in the circulation [13]. ML may be involved in the development of hard tissues, as bone and teeth [14]. ML increases alkaline phosphatase activity, dentin sialoprotein expression and mineralized matrix formation, all of them involved in dentin remineralization. ML may also regulate dentin formation and tooth development [15]. The generation of reactive oxygen species is always associated with inflammation. It has been demonstrated that, in several endodontic pathologies such as periapical abscess and pulpitis, oxidative stress is an important pathogenetic mechanism [1]. The free radicals that generate reactive oxygen or nitrogen species are considered to be highly destructive, but directly neutralized by ML [12].

As stated, ML has been used because of its anti-inflammatory, antioxidant and free-radical-scavenger properties [16,17] and cytoprotective actions [18,19]. A decline in the production of inflammatory mediators, by regulating NF-kB activity, occurs when there is high concentration of ML and contributes to signaling pathway. Although the beneficial effects of ML on periodontal regeneration has been demonstrated in gingival fibroblasts and *in vivo* and *in vitro* animal models [18], its effects in radicular dentin regeneration have not been reported yet. The circulating half-life of ML is approximately 23 min [20]. Hence, few authors have recommended the use of carriers in ML in order to release it gradually and increase the half-life in the tissues. Constant release of ML by the use of poly-lactic-co-glycolic acid microspheres has been demonstrated to differentiate human mesenchymal stem cells into osteoblasts. Novel ML delivery systems such as ML microspheres and bone-regenerating scaffolds have shown great promise for use in regenerative medicine and dentistry, specifically bone-grafting procedures, to inspire new

bone formation [21], but the release kinenics in all these studies is unknown. Controlled delivery of drugs is determinant for the radicular dentin treatment trying to reinforce the tissue [22]. Currently, this can be attained as a result of the increased use of nanoparticles (NPs) and the rapid advances of nanotechnology [23,24]. Novel polymeric NPs with anionic carboxylate (*i.e.*, COO^-) groups placed along the backbone of the polymer, that may be loaded with calcium (Ca-NPs), zinc (Zn-NPs) or doxycycline (D-NPs) have been previously synthesized to favor dentin remineralization of endodontically treated teeth [4]. However, in some cases in which apical periodontitis exists it may be valuable to consider the anti-inflammatory, antioxidant and possible remineralizing effects exerted by ML.

Histomorphometric, physical, chemical and mechanical analysis of dentin performance under the administration of exogenous melatonin would be very helpful to tentatively elucidate and confirm the therapeutic role of melatonin in dentin strengthening. Thereby, the present study was aimed to examine the possibility that melatonin might exert its influence on root dentin remineralization. Hence, the purpose of this investigation was to evaluate remineralization and dentin permeability after dentin infiltration with experimental ML-loaded NPs before the endodontic sealer placement. The tested null hypothesis was that melatonin-doped NPs application did not affect, at the short term or overtime, dentin micropermeability, neither remineralization of the endodontically treated radicular dentin.

2. Materials and Methods

2.1. Nanoparticles fabrication

PolymP-*n* Active nanoparticles (NPs) (NanoMyP, Granada, Spain) were obtained through polymerization precipitation. In order to control the process of precipitation, a thermodynamic approach has been used: the Flory-Huggins model based on the Hansen

solubility parameters. The model was developed based on the growth of polymeric chains and solvent molecules interactions by hydrogen-bonding, polar and dispersion forces [25]. The NPs are designed with 2-hydroxyethyl methacrylate as the backbone monomer, the methacrylic acid as the functional monomer and ethylene glycol dimethacrylate as the cross-linker. NPs were functionalized with melatonin. The NPs ML loading process was conducted via immersion of 150 mg of NPs in aqueous solutions of 15 mL of melatonin solutions (containing 50 mg of melatonin) for 2 h at room temperature under constant shaking. The NPs were then left at room temperature until de solvent was completely evaporated, ensuring that all the melatonin remains adhered to the NPs. NPs were resuspended in distilled water at a concentration of 10 mg/mL. To ascertain melatonin liberation profile, HPLC was used. To do this, melatonin was extracted with trichloromethane, and evaporated the organic phase to dryness using a SPD 2010 Speed Vac System (Fisher Scientific, Madrid, Spain). The samples were then analysed by HPLC (Shimadzu Europe GmbH, Duisburg, Germany) using a Waters Sunfire C18 column (150 × 4.5 mm, 5 μm). Melatonin fluorescence was measured using a Shimadzu RF-10A XL fluorescence detector (Shimadzu Europe GmbH, Duisburg, Germany) with 285-nm excitation and 345-nm emission wavelengths [26]. Three different Eppendorf tubes containing 1 mL of the Melatonin-NPs suspension (at a concentration of 10 mg/mL) were stored at 37 °C. After 24h, suspensions were centrifuged and the particles were separated from the supernatant. An aliquot of each supernatant was analyzed for melatonin concentration. NPs were washed and 1 mL of fresh distilled water was used to resuspend the NPs at 10 mg/mL until the next supernatant collection. Six different time-points were tested: 24h, 48h, 3d, 7d, 14d, and 28d. The experiment was conducted in triplicate. Two NPs-based groups were established, undoped-NPs and ML-doped NPs (ML-NPs).

2.2. Teeth specimen preparation and nanoparticles application

Forty-eight human mandibular premolars were obtained from donors (18-25 yr of age) with single roots and vital pulp, extracted for periodontal or orthodontic reasons and without caries lesions. The informed consent for inclusion was obtained from all subjects before their participation in the study. The procedure was undertaken following the Declaration of Helsinki, and the approval of the protocol was carried out by the Institution Review Board (#405/CEIH/2017). A random selection procedure was realized to select the teeth samples and they were conserved at 4 °C in 0.5% chloramine T bacteriostatic/bactericidal solution for up to 1 month. The decoronation of the teeth was realized with a low-speed diamond saw (Accutom-50 Struers, Copenhagen, Denmark), and the length of the root was standardized to approximately 12 mm and radiographed at two angulations to check the presence of a single canal. The treatment of the root canal began with the use of Gates Glidden drills (Dentsply Maillefer, Ballaigues, Switzerland), size 2 and 3, to shape the roots coronal third part. Subsequently, a size 15 Flex-o-file (Dentsply Maillefer, Ballaigues, Switzerland) was used to achieve a canal patency. The working length was recorded, and it was established 0.5 mm shorter than apical foramen. ProTaper nickel-titanium rotary instruments (Dentsply Maillefer, Ballaigues, Switzerland) up to size F4 were used for the final instrumentation. At each instrument change, the root canal was irrigated by means of a 27-gauge needle with 0.5 mL of 5% sodium hypochlorite (NaOCl, Panreac, ref. n. 212297), while at the end of canal instrumentation 0.5 mL of a 17% EDTA solution were used for 3 min (MD-Cleanser, Meta Biomed, Chungbuk, Republic of Korea) to remove the smear layer [27].

Each specimen was finally irrigated with 0.5 mL of 5% NaOCl for 1 min, followed with distilled water for one more minute, and dried with paper points (Dentsply Maillefer). The same operator conducted all procedures. The specimens were randomly separated in 3 groups (n = 10): (i) Control group, (ii) Undoped NPs group, and (iii) ML-NPs doped

group. 100 µl of the two different NPs suspensions in ethanol at 10 mg/mL were introduced into the teeth roots using a sterile micropipette. It was left undisturbed for 10 min. Then, the solvent excess was removed by gently blowing with the air syringe until evaporation, without desiccate the dentin. In one of groups, NPs were not applied (control group). Afterwards, in all groups, AH-Plus sealant cement (Dentsply Maillefer, Ballaigues, Switzerland) were introduced into the root using a lentulo spiral and it was compacted into the radicular canal with an endodontic plugger. Immediately, one size 30 guttapercha (guttacore –GC-) cone (Dentsply Maillefer, Ballaigues, Switzerland) was placed and compacted into the canal to working length, in all groups. The excess of gutta-percha and/or cement was removed from the coronal portion of the root canal, and a 3 mm space was created to insert the fluid filtration device. The space was filled with Cavit (ESPE, 3M, St. Paul, MN, USA) as a provisional restoration [28]. The adequate obturation of the material along the root canal and the voids absence was evaluated with two angulations radiographs [28–30].

2.3. Sealing ability trough the fluid filtration system

After storing the filled root canals in simulated body fluid solution [SBFS: NaCl, $NaHCO_3$, KCl, K_2HPO_4, $MgCl_2$, $CaCl_2$, and $(CH_2OH)_3$ CNH_2/HCl (6 N) to buffer the pH (7.4)], 10 teeth from each group (n=30) were coated with two layers of varnish [31] up to 2 mm from the root apex. After the removal of the provisional restoration, the coronal part was bound to a plexiglass support with cyanoacrylate adhesive (Rocket, Corona, CA, USA). A 18-gauge needle penetrated 2 mm into the root coronal piece through the Plexiglas support. The other end of the 18-gauge needle was inserted into an 18-gauge polyethylene tubing (R-3603, Tygon, Paris, France) to assess the filled roots microfiltration. A liquid flow sensor (ASL 1600, Sensirion, Staefa, Switzerland) connected between the root specimen and the source of hydraulic pressure was employed

to quantify the filled root canals fluid flow. A syringe suspended 70 cm above the sensor and filled with 60 mL of deionized water generated a constant hydraulic pressure of 6.86 kPa. The specimens were stored in SBFS and the medium was refreshed every 2 weeks. The rest of the fluid flow method of the filled root canals was assessed as in Toledano et al. [32] at different storage times (24 hours, 1 week, 3 months and 6 months) (Fig. S1).

2.4. Nanoindentation and AFM analysis

Eighteen teeth were employed for this part of the study. Half of the specimens were studied at 24 h of storage, while the other half was analyzed after 6 months. To isolate regions in the cervical and apical root dentin, two radicular disks were obtained from each root (13.5 and 4.5 mm respectively, above apex), by splitting perpendicularly to their long axis into 1 mm (±0.1 mm) thick slices (Fig. S1). The crowns were discarded at the cement-enamel junction, using a water-cooled diamond saw (Accutom-50 Struers, Copenhagen, Denmark). Two samples slabs with a 1 mm thickness were obtained sectioning bucco-lingually the root canal to examine cervical and apical areas (Fig. S1b). 800 up to 4000 grit SiC abrasive papers were used to polish the surfaces. The final polishing steps were done by using diamond pastes through 1 µm down to 0.25 µm (Struers LaboPol-4; Struers GmbH, Hannover, Germany) (Fig. S1). After each polishing step, samples were treated with deionized water for 5 min in ultrasonic bath (Model QS3, Ultrawave Ltd, Cardiff, UK).

2.4.1. Young's modulus and Nano-DMA analysis

A Hysitron Ti-750D TriboIndenter indentation system (Hysitron Inc., Minneapolis, MN) equipped with a commercial nano-DMA package was employed. A Berkovich (three sides pyramidal) diamond tip (tip radius ~20 nm) was used as the nanoindenter. The calibration of the nanoindenter tip was performed over a fused quartz sample. A quasistatic force setpoint of 5 µN was used. The calibration-reduced modulus value of

1.1400E+03 N/mm^2 was employed to obtain the best-fit spherical radius (150 nm). Ten intertubular dentin indentations were performed on each specimen at 20 µm next to radicular canal (inner zone) (Fig. S1b). A load of 4000 nN and a time function of 10 s were used to execute the indentations. The tip pressed progressively over the sample (at a constant rate) up to a peak load of 4000 µN. The indentations were performed in an hydrated condition. A drop of ethylene glycol was put over the dentin surfaces to avoid water evaporation during a 25-to-30-min scanning period. The rest of the process was performed as in Toledano et al. [32] and Toledano-Osorio et al. [33].

Dentin disks were also subjected to nano-DMA analyses. A dynamic (oscillatory) force of 2 µN was superimposed on the quasistatic signal at a frequency of 200 Hz. Based on a calibration-reduced modulus value of 69.6 GPa for the fused quartz, the best-fit spherical radius approximation for tip was found to be 150 nm, for the selected nano-DMA scanning parameters. Modulus mapping was conducted by imposing a quasistatic force setpoint, Fq=2 µN, to which it was superimposed a sinusoidal force of amplitude FA=0.10 µN and frequency f=100 Hz. The resulting displacement (deformation) at the site of indentation was monitored as a function of time. Data from regions, approximately 20×20 µm in size, were collected using a scanning frequency of 0.2 Hz. Specimens were scanned under a hydrated condition. In order to accomplish for this purpose, samples were stored in PBS after polishing to maintain the hydration. Both Young's modulus (*Ei*) and tan delta (δ) were calculated.

2.4.2. Atomic Force Microscopy (AFM) and nanoroughness assessments

Topography mappings were obtained with an atomic force microscope (AFM Nanoscope V, Digital Instruments, Veeco Metrology group, Santa Barbara, CA, USA). The images were obtained, in a fully hydrated state, inside a fluids cell of the AFM using the tapping mode with a calibrated vertical-engaged piezo-scanner (Digital Instrument, Santa

Barbara, CA, USA). An oscillating cantilever with a 10 nm radius silicon nitride tip (Veeco) contacted intermittently with the dentin surface at the lowest point of the oscillation. Changes in vertical position of the AFM tip at resonance frequencies near 330 kHz provided the height of the images registered as bright and dark regions. 5 x 5 and 2 x 2 µm digital images were recorded with a slow scan rate (0.1 Hz). For each image, 5 randomized boxes (1 x 1 µm) were created to examine the nanoroughness at 24 h and 6 m of storage. Nanoroughness (SRa, in nanometers) was measured with proprietary software (Nanoscope Software, version V7). The rest of the procedure was as in Toledano et al. [32].

2.5. Statistical analysis

Microleakage, Young's modulus, tan delta, and nanoroughness were statistically analyzed. As the normality and homoscedasticity conventions of the data were valid, ANOVA and Student-Newman-Keuls multiple comparison tests were employed, with statistical significance preset at $p<0.05$. Microleakage, Young's modulus, tan delta, and nanoroughness were considered dependent variables in each ANOVA model. NPs, storage time, and dentin zone (cervical/apical) were independent influencing factors. Interactions between factors were included in the analysis.

2.6. Raman spectroscopy

The same AFM-analyzed dentin surfaces were subsequently studied with Raman spectroscopy. For this analysis, it was employed a dispersive Raman spectrometer/microscope (Horiba Scientific Xplora, Villeneuve d´Ascq, France) with a 785-nm diode laser through a X100/0.90 NA air objective and with 500 µm pinhole (which means a spatial resolution of 785 nm, approximately). The spectrometer was equipped with a CCD detector (DR-324B-FI-327, Andor Technology LTD, UK). The 785 nm laser was used with 100X objective, and the spectral resolution of the system was 2

cm^{-1}. Two surface areas of 12x12 µm were mapped at dissimilar sites for each sample at X and Y axis with a 0.5 µm spacing (625 points per map) and each spectrum was measured by using 2s acquisition time with 2 accumulations. Chemical mapping was submitted to K-means cluster (KMC) analysis using the multivariate analysis tool (ISys® Horiba), which includes statistical pattern to derive the independent clusters. The K-means clustering is a method of analysis based on a centroid model which aims to partition "n" observations into "k" clusters in which each observation belongs to the cluster with the nearest mean. The natural groups of components (or data) based on some similarity and the centroids of a group of data sets were found by the clustering algorithm once calculated by the software and the Hierarchical Cluster Analysis (HCA). The observed spectra were described at 400-1700 cm^{-1} with 10 complete overlapping Gaussian lines, suggesting homogeneous data for further calculations [34]. Each cluster biochemical content was examined though the average cluster spectra. Using the Hierarchical Cluster Analysis (HCA) and the algorithm calculated by the software, the natural groups of components (or data) based on some similarity and the centroids of a group of data sets was found. At this point, the dentin mineral component was assessed studying the relative presence of mineral, *i.e*, the phosphate (960 cm^{-1}) peak and area and the relative mineral concentration of phosphate (PO_4^{3-}) referred to phenyl (RMC_p), the stoichiometric HAp (963 cm^{-1}), the carbonate peak (1070 cm^{-1}), and the crystallinity of biological apatites by the value of the 1020/1030 ratio intensity (1020 cm^{-1}, nonstoichiometric apatites containing HPO_4^{2-}, CO_3^{2-}, and vacancies; 1030 cm^{-1}, stoichiometric apatites) [35,36]. The dentin organic component was analyzed examining the crosslinking at 1032 cm^{-1} (pyridinium ring vibration), the nature and secondary structure of collagen (C-C stretch of hydroxyproline, C-C Hydroxilated proline, collagen and lipids and proteins) and the proteoglycans [37,38].

2.7. Field Emission Scanning Electron Microscopy (FESEM)

Dentin surfaces were then fixed for 24 h in a 2.5% glutaraldehyde solution in 0.1 mol/L sodium cacodylate buffer. To observe the samples with a field emission scanning electron microscope (FESEM Gemini, Carl Zeiss, Oberkochen, Germany), they were exposed to critical point drying (Leica EM CPD 300, Wien, Austria) and sputter-coated with carbon by means of a sputter-coating Nanotech Polaron-SEMPREP2 (Polaron Equipment Ltd., Watford, UK). An X-ray detector system (EDX Inca 300, Oxford Instruments, Oxford, UK) attached to the FESEM realized an energy-dispersive analysis at designated points.

3. Results

3.1. Melatonin liberation profile

The melatonin liberation profile curve is shown in Fig. S2. It corresponded with the following amount of melatonin expressed in mg/ml at each time point: 24 h, 1.85; 48 h, 0.65; 3 d, 0.37; 7 d, 0.13; 14 d, 0.13; 28 d, 0.033.

3.2. Sealing ability trough the fluid filtration system

The fluid filtration rate (µL min^{-1}) at distinct storage time for all groups is shown in Fig. 1. Significant differences ($P<0.05$) were found between groups. All groups showed the same microleakage values after 24 h and 1 w of storage. Control samples promoted the highest microleakage values among groups, at 6 m time point; specimens treated with undoped NPs and ML-NPs performed similar after 6 m storage.

3.3. Nanoindentation

Mean and SD of the modulus of Young (*Ei*) at the two different dentin disks (cervical and apical) are represented in Fig. 2a. All specimens, regardless the group, performed similar when cervical root dentin was analyzed at 24 h of storage. Samples treated with undoped NPs attained higher *Ei* than the rest of the groups at apical root dentin. After 6 m of storage all NPs-treated groups attained higher *Ei* than the control group. Control samples showed

an *Ei* decrease over time, irrespective of the dentin location. Cervical dentin treated with undoped NPs maintained its *Ei* after 6 m of storage, but *Ei* decreased at apical dentin. When ML-NPs were used, *Ei* was similar over time, regardless the dentin location. At 6 m of storage tan delta assessed at cervical dentin in control specimens and those treated ML-NPs obtained higher values than samples treated with undoped NPs. At apical dentin, specimens treated with ML-NPs attained the highest tan delta values (Fig. 2b).

3.4. Atomic Force Microscopy (AFM) and nanoroughness assessments

Control specimens and ML-NPs treated ones attained lower SRa values than those treated with undoped NPs, at both cervical and apical root dentin, after 6 m of storage (Fig. 2c). At the apical half of radicular dentin, samples treated with ML-NPs decreased their roughness values overt time. Samples treated with undoped NPs did not modify their SRa values over time (Fig. 2c). AFM analysis, in Fig. 3, permitted to observe dentin control surfaces showing open dentinal tubules with numerous microporosities (Figs. 3a, 3d). Undoped NPs on dentin provoked filled or open dentinal tubule entrances and sights of stress concentration affecting intertubular and peritubular dentin structures with microcraking (Figs. 3b, 3e). Smoother dentin surfaces, strongly mineralized, were observed when ML-NPs were applied on radicular dentin (Figs. 3c, 3f). At 24 h storage, control samples showed both peritubular and intertubular dentin clearly identified (Figs. S3a, S3d). Tubules appeared completely, partially occluded or empty when undoped NPs were applied on dentin (Figs. S3b, S3e). Peritubular, intertubular and intratubular mineralization characterized the application of ML-NPs on radicular dentin (Figs. S3c, S3f).

3.5. Raman spectroscopy

ML-NPs-treated samples at both cervical and apical root dentin achieved the highest phosphate peak (961 cm^{-1}) intensity and area, *i.e*, higher mineralization among groups, at

6 m (Table 1) (Figs. 4c, 4f). After 6 m of storage, the carbonate peak (1070 cm^{-1}) also showed its highest value at both cervical and apical dentin (Table 1). Stoichiometric HAp (963 cm^{-1}) and crystallinity (ratio 1020/1030) obtained their highest peak values after using ML-NPs in dentin, regardless the zone of application (Table 1). HCA Raman images (clusters) and results (centroids) (Fig. S4) achieved at ML-NPs-treated specimens after 6 m of storage showed remarkable higher phosphate peaks and different variances, both corresponding to the three distinguishable centroids (HCA_1, HCA_2 and HCA_3), in comparison with the those obtained when undoped-NPs were utilized. Mineralization related to the relative mineral concentration (RMC) linked to phenyl group (1003 cm^{-1}) at cervical dentin when ML-NPs were used was higher than when samples were treated with undoped NPs (Table 1). The highest cross-linking of collagen was attained by samples treated with ML-NPs at both cervical and apical dentin after 6 m of storage (Table 1). The highest ratio proline/hydroxyproline, indicative of the quality and nature of collagen was obtained by samples treated with ML-NPs, regardless the type of dentin, at 6 m time point (Table 1). The highest peaks of collagen (937 cm^{-1}), lipids/proteins CH_2 (1448 cm^{-1}) and proteoglycans (1062 cm^{-1}) bands were achieved by samples treated with ML-NPs regardless the kind of radicular dentin, at 6 m of storage (Table 1).

3.6. Field Emission Scanning Electron Microscopy (FESEM)

After 6 m of storage, FESEM analysis was performed at radicular dentin interfaces. Gaps were shown at the canal sealer-dentin interface when control specimens (Figs. S5a, S5b) and those treated with undoped-NPs were observed (Figs. S5c, S5d). Samples treated with undoped NPs permitted to see the NPs intimately close to the collagen fibers, and tubules appeared with a robust peritubular dentin ring. Specimens treated with ML-NPs displayed a generalized mineralization pattern, covering both intertubular and peritubular dentin,

and totally occluding the dentinal tubules. Peritubular dentin turned up strongly mineralized. Dentinal tubules were hardly distinguised (Figs. 5e, 5f).

4. Discussion

ML-NPs achieved root dentin sealing and remineralization, as they occlude dentinal tubules and attain reinforcement of the radicular dentin structure, but did not affect fluid filtration at the dentin interface. Therefore, the null hypothesis that ML-NPs application did not affect, at the short term or overtime, dentin micropermeability neither remineralization of the endodontically treated radicular dentin, must be partially rejected. NPs application (undoped or ML-doped) reduced liquid flow if compared to control group. Commonly, micropermeability and microleakage are associated and both correlate with the presence of porosities [39]. The enhancement of sealing ability obtained by ML-NPs and undoped NPs treated in root dentin (Fig. 1), after 6 m of storage, is associated to the hydroxyapatite formation that would close pores, voids and capillary channels [40] (Figs. S3b, S3c, S3e, S3f) through calcium-phosphate salts deposits. Firm mineral segments around and within the dentinal tubules were shown in ML-NPs treated samples, even after 24 h time point (Figs. 5a-d). The entrances of dentin tubules were not able to be observed at 6 m of storage (Figs. 5e, 4f).

Though both types of NPs provided similar values of Young's modulus at 6 m storage, ML-NPs can be considered as a drug of long-lasting or durable effect, meanwhile undoped NPs provoked a treatment of unstable or degraded effect (Fig. 2a). This decline in mechanical properties is normally linked to low chemical stability leading to an ion-rich environment, likely associated with an improved bioactivity and increased solubility [41,42]. Relative or partial dentin remineralization after undoped-NPs application has been proved in the present research, as some demineralized collagen fibers and empty dentinal tubules, after treating root dentin, were observed at 6 m of storage (Figs. 3e, S5c,

S5d). Occluded tubules may affect dentin mechanical properties [33,43]. AFM analysis permitted to observe totally filled tubules after using ML-NPs (Fig. 3c). Microcracking (Fig. 3e) have been shown in unfilled tubules. Otherwise, filled tubules can act as uncracked-ligament bridging [44,45]. The highest tan delta values (Fig. 2b) that dentin samples treated with ML-NPs attained, have become, potentially, associated to the presence of intratubular mineral precipitation [33] (Figs. 5a-d, 3c). It reflects how well a material can get rid of the energy. The lower tan delta (0.021, attained after undoped-NPs application at apical dentin), the greater the proportion of energy available in the system for recoil and/or failure [46]. As a result, lower levels of stored energies at the interface can be observed after 6 months of SBFS storage, when radicular dentin was treated with ML-NPs at the apical half (0.33). Multiple stress concentration, strain and deformations occur at cervical root dentin [47], meanwhile apical dentin has shown the maximal tensile strength and a strong reduction of fracture strength after instrumentation [48,49]. The strain distribution indicates the stiffness of the tooth as force bearing tissue during biting [50,51]. In addition, intrafibrillar remineralization is commonly associated to mineral maturation and decreases in roughness values [52]. Additionally, at the inner region of root dentin, increased mineralization has been detected at the inner region of root dentin when remineralizing strategies are implemented. This zone is reinforced at the expense of an increase in Young's modulus, complex modulus and sealing ability [3]. Therefore, an increase of the overall fracture resistance of the root can be inferred [53]. Melatonin, as a result, may be a potent biomimetic agent in restoring oral hard tissues [54].

Dentin surfaces treated with ML-NPs obtained the highest mineralization observed after Raman analysis, as both phosphate bands (960 cm^{-1}) (peak and area) and the relative mineral concentration attained the highest values when NPs were doped with melatonin (Table 1). This meant major presence of calcium phosphate (Figs. 3, 4e, 4f) that

precipitated in three different type of HAp crystals, from a biochemical standpoint, more homogeneous and similar in proportion than when undoped NPs were used (Figs. S4a-d). The observed rise of minerals became associated, at the same time, to the highest crosslinking (1032 cm^{-1}) of collagen that was achieved by ML-NPs treated samples (Table 1). A growth in crosslinking of collagen usually occurs after mineral precipitation [55,56] that improves sealing ability (Fig. 1), and could be the base for the enhancement of mechanical properties of dentin [32]. The rise in the modulus of Young has become to be associated to an increase of the stoichiometric HAp, crystallinity and maturity [57], which were augmented when samples were treated with ML-NPs. In calcified tissues, crystallinity, low nanoroughness [52] and improved tissue maturation (Fig. 2) are associated, altogether linked to intrafibrillar remineralization and improved mechanical properties [43,58], *e,g*, high Young´s modulus (Table 1, Fig. 2a).

ML (physiological dose range) induced a dose-dependent reduction in dental papilla cell proliferation, dentin sialoprotein expression, and mineralized matrix formation *in vitro* [14]. Melatonin has been show to increase alkaline phosphatase [59]. Tissue alkaline phosphatase is a zinc-metalloenzyme that protect the collagen [60] and hydrolyzes a big spectrum of phosphate monoesters [61,62]. Around the collagen fibrils and at high phosphate concentration, unstable and non-crystalline amorphous complexes, calcium phosphate and calcium pyrophosphate, are deposited [63,64]. It is known that dentin retains the alkaline phosphatase and other enzymes "fossilized" [65], thus impeding the complete remineralization. Even more, melatonin has been proved to stimulate the proliferation and synthesis of type I collagen [12,16], which is necessary for the adhesion of the infiltrated NPs, self-protection of the collagen web and further mineral precipitation [66]. In the present research, collagen (937 cm^{-1}), hydroxyproline (871 cm^{-1}) and

hydroxylated proline (920 cm^{-1}) bands were higher in dentin specimens treated with ML-NPs than in the rest of the groups, regardless of the dentin zone (Table 1).

Biological apatite contains substantial amounts of carbonate and is calcium deficient [67]. The increase of the carbonate peak (1070 cm^{-1}) in radicular dentin when compared with the rest of the groups reflects a higher presence of carbonate apatite in samples treated with ML-NPs (Table 1). Carbonated apatite is an amorphous precursor of HAp [67]. This amorphization was likely associated to the intake of carbonate as substituent for PO_4^3 in the apatite lattice. Changes in the spectral region of carbonate content have been ascribed to either growth of a carbonate peak or changes in the phosphate peak in response to the presence of carbonate in the lattice [68]. The presence of a prominent carbonate band around 1070 cm^{-1}correlated with the increased degree of carbonate substitution in the lattice structure of apatite [69], and match with the broad augmentation of the full-width half-maximum (FWHM) of the phosphate v_1 peak (at ca. 960 cm^{-1}) [70]. Signals corresponding to proteoglycans augmented in samples treated with ML-NPs (Table 1). Glycosaminoglycans and proteoglycans participate in biomineralization *via* the function of the highly negatively charged glycosaminoglycan side chains in engaging calcium ions, leading a biological signaling role [58,71,72]. Melatonin-doped NPs gave rise to an increase of lipids peak (1448 cm^{-1}) (Table 1) in a substratum, the endodontium, where free lipid concentrations are quite low [1]. The lipophilic properties of melatonin will help to enter the subcellular compartment and display its role as antioxidant and immunomodulatory properties [1]. Further research is needed to develop this focus.

The highest relative mineral concentration (RMC) (34.21) (Table 1) and the *Ei* decrease at 6 months of storage (34%) (Fig. 2a) that was attained after treating dentin with undoped-NPs means that the relative degree of mineral gain was at the expenses of non-functional dentin remineralization, *i.e*, extrafibrillar mineralization [58]. The decrease of

the Young modulus in control samples and in those treated with undoped-NPs, especially at apical dentin, may be interpreted as a sight of dentin demineralization and further degradation [63] (Fig. 2a), indicating scarce remineralization potential at the intrafibrillar compartment after 6 m of storage. Structural porosity, micropermeability, microleakage, demineralization and collagen degradation are closely related [63]. Thereby, ML-NPs must be presented as a feasible option to obtain radicular dentin sealing and remineralization, as they produce the occlusion of dentinal tubules and the reinforcement of the dentin structure. Melatonin liberation was maintained even after 28 d (0.03 mg/ml) (Fig. S2), more than enough quantity to undertake and accomplish the objectives that were proposed in the present research. Furthermore, the melatonin release from NPs would *in situ* display its anti-inflammatory, antioxidant and free-radical-scavenger properties at the affected root dentin [16]. It has been demonstrated that oxidative stress is an important pathogenetic mechanism in several endodontic pathologies, such as periapical abscess and pulpitis [1]. Oxidative stress levels depend on one hand on the bacterial infection-related inflammation and on the other hand, the protective power of the antioxidative system [1]. Prooxidant and antioxidant levels are normally balanced in the body, including the oral cavity. Moreover, it should be considered that non-released melatonin that remained bonded to NPs may also be bioactive. More research to lastly prove definitive clinical advantages in patients with endodontic needs using melatonin-doped nanoparticles is encouraged. There are some limitations to this experiment. It does not test the long-term effect of NPs, as a 12 and 24 m study. X-ray micro-computed tomography and X-ray fluorescence microscopy studies should be oriented in future research, in order to include morpho-physico-chemically evaluation of these treated surfaces. The tentative combination of zinc or doxycycline load NPs with ML-NPs could

represent a new challenge for a remineralizing, antimicrobial, and anti-inflammatory therapy in root canal dentin.

3. Conclusions

Sealing and remineralization of the radicular dentin was not efficient at the control group, as a high quantity of the dentin tubules remained open and the highest microleakage was obtained over time. The use of melatonin promoted total occlusion of dentinal tubules and an almost complete reduction of fluid flow, exhibiting the highest sealing ability among groups. Non-functional remineralization was produced at the control group, based on the new deposits of immature and imperfect nanocrystallite dentin structures. The low microleakage values attained by samples treated with both undoped NPs and ML-NPs were consistent with the highest modulus of Young. Advanced functional dentin remineralization and higher crystallinity was achieved and preserved with the use of ML-NPs. After 6 months, radicular dentin treated with undoped-NPs showed lower crystallinity than dentin treated with ML-NPs, providing more amorphous phase in the ultrafine nano-crystalline hydroxyapatite. As a result, ML-NPs might be considered as a feasible treatment for radicular dentin reinforcement in endodontics, after doing additional experimental tests to overcome the restrictions of the present *in vitro* study.

Acknowledgements

This work was funded by: 1) the Ministry of Economy and Competitiveness and European Regional Development Fund (MAT2017-85999P MINECO/AEI/FEDER/UE).

References

[1] Vengerfeldt V, Mändar R, Saag M, Piir A, Kullisaar T. Oxidative stress in patients with endodontic pathologies. JPR 2017;Volume 10:2031–40. https://doi.org/10.2147/JPR.S141366.

[2] Yoo Y-J, Oh J-H, Zhang Q, Lee W, Woo KM. Dimethyloxalylglycine-embedded Poly(ε-caprolactone) Fiber Meshes Promote Odontoblastic Differentiation of Human Dental Pulp-derived Cells. J Endod 2018;44:98-103.e1. https://doi.org/10.1016/j.joen.2017.09.002.

[3] Toledano M, Osorio R, Vallecillo-Rivas M, Osorio E, Lynch CD, Aguilera FS, et al. Zn-doping of silicate and hydroxyapatite-based cements: Dentin mechanobiology and bioactivity. J Mech Behav Biomed Mater 2021;114:104232. https://doi.org/10.1016/j.jmbbm.2020.104232.

[4] Toledano M, Osorio E, Aguilera FS, Muñoz-Soto E, Toledano-Osorio M, López-López MT, et al. Polymeric nanoparticles for endodontic therapy. J Mech Behav Biomed Mater 2020;103:103606. https://doi.org/10.1016/j.jmbbm.2019.103606.

[5] Kinney JH, Nalla RK, Pople JA, Breunig TM, Ritchie RO. Age-related transparent root dentin: mineral concentration, crystallite size, and mechanical properties. Biomaterials 2005;26:3363–76. https://doi.org/10.1016/j.biomaterials.2004.09.004.

[6] Gandolfi MG, Prati C. MTA and F-doped MTA cements used as sealers with warm gutta-percha. Long-term study of sealing ability. Int Endod J 2010;43:889–901. https://doi.org/10.1111/j.1365-2591.2010.01763.x.

[7] Torabinejad M, Watson TF, Pitt Ford TR. Sealing ability of a mineral trioxide aggregate when used as a root end filling material. J Endod 1993;19:591–5. https://doi.org/10.1016/S0099-2399(06)80271-2.

[8] Monticelli F, Sword J, Martin RL, Schuster GS, Weller RN, Ferrari M, et al. Sealing properties of two contemporary single-cone obturation systems. Int Endod J 2007;40:374–85. https://doi.org/10.1111/j.1365-2591.2007.01231.x.

[9] Hakki SS, Bozkurt BS, Ozcopur B, Gandolfi MG, Prati C, Belli S. The response of cementoblasts to calcium phosphate resin-based and calcium silicate-based commercial sealers. Int Endod J 2013;46:242–52. https://doi.org/10.1111/j.1365-2591.2012.02122.x.

[10] Toledano-Osorio M, Osorio R, Aguilera FS, Medina-Castillo AL, Toledano M, Osorio E, et al. Polymeric nanoparticles protect the resin-dentin bonded interface from cariogenic biofilm degradation. Acta Biomaterialia 2020;111:316–26. https://doi.org/10.1016/j.actbio.2020.05.002.

[11] Shino H, Hasuike A, Arai Y, Honda M, Isokawa K, Sato S. Melatonin enhances vertical bone augmentation in rat calvaria secluded spaces. Med Oral 2016:e122–6. https://doi.org/10.4317/medoral.20904.

[12] Meenakshi SS, Malaiappan S. Role of melatonin in periodontal disease - A systematic review. Indian J Dent Res 2020;31:593–600. https://doi.org/10.4103/ijdr.IJDR_227_18.

[13] Acuña-Castroviejo D, Rahim I, Acuña-Fernández C, Fernández-Ortiz M, Solera-Marín J, Sayed RKA, et al. Melatonin, clock genes and mitochondria in sepsis. Cell Mol Life Sci 2017;74:3965–87. https://doi.org/10.1007/s00018-017-2610-1.

[14] Liu J, Huang F, He H-W. Melatonin Effects on Hard Tissues: Bone and Tooth. Int J Mol Sci 2013;14:10063. https://doi.org/10.3390/ijms140510063.

[15] Liu J, Zhou H, Fan W, Dong W, Fu S, He H, et al. Melatonin influences proliferation and differentiation of rat dental papilla cells in vitro and dentine formation in vivo by altering mitochondrial activity. J Pineal Res 2013;54:170–8. https://doi.org/10.1111/jpi.12002.

[16] Köse O, Arabaci T, Kizildag A, Erdemci B, Eminoğlu DÖ, Gedikli S, et al. Melatonin prevents radiation-induced oxidative stress and periodontal tissue breakdown in irradiated rats with experimental periodontitis. J Periodontal Res 2017;52:438–46. https://doi.org/10.1111/jre.12409.

[17] Fernández-Ortiz M, Sayed RKA, Fernández-Martínez J, Cionfrini A, Aranda-Martínez P, Escames G, et al. Melatonin/Nrf2/NLRP3 Connection in Mouse Heart Mitochondria during Aging. Antioxidants 2020;9. https://doi.org/10.3390/antiox9121187.

[18] Santos RM dos, Marani F, Chiba FY, Mattera MS de LC, Tsosura TVS, Tessarin GWL, et al. Melatonin promotes reduction in TNF levels and improves the lipid profile and insulin sensitivity in pinealectomized rats with periodontal disease. Life Sciences 2018;213:32–9. https://doi.org/10.1016/j.lfs.2018.09.056.

[19] Fernández-Gil B, Moneim AEA, Ortiz F, Shen Y-Q, Soto-Mercado V, Mendivil-Perez M, et al. Melatonin protects rats from radiotherapy-induced small intestine toxicity. PLoS One 2017;12. https://doi.org/10.1371/journal.pone.0174474.

[20] Gibbs FP, Vriend J. The half-life of melatonin elimination from rat plasma. Endocrinology 1981;109:1796–8. https://doi.org/10.1210/endo-109-5-1796.

[21] Maria S, Witt-Enderby PA. Melatonin effects on bone: potential use for the prevention and treatment for osteopenia, osteoporosis, and periodontal disease and for use in bone-grafting procedures. J Pineal Res 2014;56:115–25. https://doi.org/10.1111/jpi.12116.

[22] Yoo Y-J, Kwon I, Oh S-R, Perinpanayagam H, Lim S-M, Ahn K-B, et al. Antifungal Effects of Synthetic Human Beta-defensin-3-C15 Peptide on Candida

albicans–infected Root Dentin. J Endod 2017;43:1857–61. https://doi.org/10.1016/j.joen.2017.06.035.

[23] Chieruzzi M, Pagano S, Moretti S, Pinna R, Milia E, Torre L, et al. Nanomaterials for Tissue Engineering In Dentistry. Nanomaterials 2016;6. https://doi.org/10.3390/nano6070134.

[24] Negi H, Saikia SK, Kanaujia R, Jaiswal S, Pandey R. 3β-Hydroxy-urs-12-en-28-oic acid confers protection against ZnONPs induced adversity in Caenorhabditis elegans. Environ Toxicol Pharmacol 2017;53:105–10. https://doi.org/10.1016/j.etap.2017.05.004.

[25] Medina-Castillo AL, Fernandez-Sanchez JF, Segura-Carretero A, Fernandez-Gutierrez A. Micrometer and Submicrometer Particles Prepared by Precipitation Polymerization: Thermodynamic Model and Experimental Evidence of the Relation between Flory's Parameter and Particle Size. Macromolecules 2010;43:5804–13. https://doi.org/10.1021/ma100841c.

[26] Shen Y-Q, Guerra-Librero A, Fernandez-Gil BI, Florido J, García-López S, Martinez-Ruiz L, et al. Combination of melatonin and rapamycin for head and neck cancer therapy: Suppression of AKT/mTOR pathway activation, and activation of mitophagy and apoptosis via mitochondrial function regulation. J Pineal Res 2018;64:e12461. https://doi.org/10.1111/jpi.12461.

[27] O'Connell MS, Morgan LA, Beeler WJ, Baumgartner JC. A comparative study of smear layer removal using different salts of EDTA. J Endod 2000;26:739–43. https://doi.org/10.1097/00004770-200012000-00019.

[28] Mestres G, Aguilera FS, Manzanares N, Sauro S, Osorio R, Toledano M, et al. Magnesium phosphate cements for endodontic applications with improved long-term sealing ability. Int Endod J 2014;47:127–39. https://doi.org/10.1111/iej.12123.

[29] Monticelli F, Osorio R, Toledano M, Ferrari M, Pashley DH, Tay FR. Sealing properties of one-step root-filling fibre post-obturators vs. two-step delayed fibre post-placement. J Dent 2010;38:547–52. https://doi.org/10.1016/j.jdent.2010.03.014.

[30] Vizgirda PJ, Liewehr FR, Patton WR, McPherson JC, Buxton TB. A comparison of laterally condensed gutta-percha, thermoplasticized gutta-percha, and mineral trioxide aggregate as root canal filling materials. J Endod 2004;30:103–6. https://doi.org/10.1097/00004770-200402000-00010.

[31] Bouillaguet S, Shaw L, Barthelemy J, Krejci I, Wataha JC. Long-term sealing ability of Pulp Canal Sealer, AH-Plus, GuttaFlow and Epiphany. Int Endod J 2008;41:219–26. https://doi.org/10.1111/j.1365-2591.2007.01343.x.

[32] Toledano M, Muñoz-Soto E, Aguilera FS, Osorio E, González-Rodríguez MP, Pérez-Álvarez MC, et al. A zinc oxide-modified hydroxyapatite-based cement favored sealing ability in endodontically treated teeth. J Dent 2019;88:103162. https://doi.org/10.1016/j.jdent.2019.06.009.

[33] Toledano-Osorio M, Osorio E, Aguilera FS, Luis Medina-Castillo A, Toledano M, Osorio R. Improved reactive nanoparticles to treat dentin hypersensitivity. Acta Biomater 2018. https://doi.org/10.1016/j.actbio.2018.03.033.

[34] Ager JW, Nalla RK, Breeden KL, Ritchie RO. Deep-ultraviolet Raman spectroscopy study of the effect of aging on human cortical bone. J Biomed Opt 2005;10:034012. https://doi.org/10.1117/1.1924668.

[35] Toledano M, Pérez-Álvarez MC, Aguilera FS, Osorio E, Cabello I, Toledano-Osorio M, et al. A zinc oxide-modified hydroxyapatite-based cement facilitated new crystalline-stoichiometric and amorphous apatite precipitation on dentine. Int Endod J 2017;50 Suppl 2:e109–19. https://doi.org/10.1111/iej.12807.

[36] Magne D, Weiss P, Bouler JM, Laboux O, Daculsi G. Study of the maturation of the organic (type I collagen) and mineral (nonstoichiometric apatite) constituents of a calcified tissue (dentin) as a function of location: a Fourier transform infrared microspectroscopic investigation. J Bone Miner Res 2001;16:750–7. https://doi.org/10.1359/jbmr.2001.16.4.750.

[37] Toledano M, Osorio E, Aguilera FS, Cabello I, Toledano-Osorio M, Osorio R. Ex vivo detection and characterization of remineralized carious dentin, by nanoindentation and single point Raman spectroscopy, after amalgam restoration. J Raman Spectrosc 2017;48:384–92. https://doi.org/10.1002/jrs.5055.

[38] Kunstar A, Leijten J, van Leuveren S, Hilderink J, Otto C, van Blitterswijk CA, et al. Recognizing different tissues in human fetal femur cartilage by label-free Raman microspectroscopy. J Biomed Opt 2012;17:116012. https://doi.org/10.1117/1.JBO.17.11.116012.

[39] Profeta AC, Mannocci F, Foxton RM, Thompson I, Watson TF, Sauro S. Bioactive effects of a calcium/sodium phosphosilicate on the resin–dentine interface: a microtensile bond strength, scanning electron microscopy, and confocal microscopy study. Eur J Oral Sci 2012;120:353–62. https://doi.org/10.1111/j.1600-0722.2012.00974.x.

[40] Gandolfi MG, Sauro S, Mannocci F, Watson TF, Zanna S, Capoferri M, et al. New tetrasilicate cements as retrograde filling material: an in vitro study on fluid penetration. J Endod 2007;33:742–5. https://doi.org/10.1016/j.joen.2007.02.008.

[41] Low I-M. Depth-Profiling of Crystal Structure, Texture, and Microhardness in a Functionally Graded Tooth Enamel. J Am Ceram Soc 2004;87:2125–31. https://doi.org/10.1111/j.1151-2916.2004.tb06369.x.

[42] Osorio R, Cabello I, Toledano M. Bioactivity of zinc-doped dental adhesives. J Dent 2014;42:403–12. https://doi.org/10.1016/j.jdent.2013.12.006.

[43] Toledano-Osorio M, Aguilera FS, Osorio R, Muñoz-Soto E, Pérez-Álvarez MC, López-López MT, et al. Hydroxyapatite-based cements induce different apatite formation in radicular dentin. Dent Mater 2020;36:167–78. https://doi.org/10.1016/j.dental.2019.11.023.

[44] Koester KJ, Ager JW, Ritchie RO. The effect of aging on crack-growth resistance and toughening mechanisms in human dentin. Biomaterials 2008;29:1318–28. https://doi.org/10.1016/j.biomaterials.2007.12.008.

[45] Shinno Y, Ishimoto T, Saito M, Uemura R, Arino M, Marumo K, et al. Comprehensive analyses of how tubule occlusion and advanced glycation end-products diminish strength of aged dentin. Sci Rep 2016;6:19849. https://doi.org/10.1038/srep19849.

[46] Espino DM, Shepherd DET, Hukins DWL. Viscoelastic properties of bovine knee joint articular cartilage: dependency on thickness and loading frequency. BMC Musculoskelet Disord 2014;15:205. https://doi.org/10.1186/1471-2474-15-205.

[47] Kaushik M, Kumar U, Sharma R, Mehra N, Rathi A. Stress distribution in endodontically treated abfracted mandibular premolar restored with different cements and crowns: A three-dimensional finite element analysis. J Conserv Dent 2018;21:557–61. https://doi.org/10.4103/JCD.JCD_206_18.

[48] Patil P, Banga KS, Pawar AM, Pimple S, Ganeshan R. Influence of root canal obturation using gutta-percha with three different sealers on root reinforcement of endodontically treated teeth. An in vitro comparative study of mandibular incisors. J Conserv Dent 2017;20:241–4. https://doi.org/10.4103/JCD.JCD_233_16.

[49] Brosh T, Metzger Z, Pilo R. Circumferential root strains generated during lateral compaction with stainless steel vs. nickel-titanium finger spreaders. Eur J Oral Sci 2018;126:518–25. https://doi.org/10.1111/eos.12569.

[50] Fujisaki K, Todoh M, Niida A, Shibuya R, Kitami S, Tadano S. Orientation and deformation of mineral crystals in tooth surfaces. J Mech Behav Biomed Mater 2012;10:176–82. https://doi.org/10.1016/j.jmbbm.2012.02.025.

[51] Toledano M, Osorio E, Aguilera FS, Toledano-Osorio M, López-López MT, Osorio R. Stored potential energy increases and elastic properties alterations are produced after restoring dentin with Zn-containing amalgams. J Mech Behav Biomed Mater 2019;91:109–21. https://doi.org/10.1016/j.jmbbm.2018.12.002.

[52] Zurick KM, Qin C, Bernards MT. Mineralization Induction Effects of Osteopontin, Bone Sialoprotein, and Dentin Phosphoprotein on a Biomimetic Collagen Substrate. J Biomed Mater Res A 2013;101:1571–81. https://doi.org/10.1002/jbm.a.34462.

[53] Toledano M, Vallecillo-Rivas M, Aguilera FS, Osorio MT, Osorio E, Osorio R. Polymeric zinc-doped nanoparticles for high performance in restorative dentistry. J Den 2021;107:103616. https://doi.org/10.1016/j.jdent.2021.103616.

[54] Cutando A, Gómez-Moreno G, Arana C, Muñoz F, Lopez-Peña M, Stephenson J, et al. Melatonin stimulates osteointegration of dental implants. J Pineal Res 2008;45:174–9. https://doi.org/10.1111/j.1600-079X.2008.00573.x.

[55] Toledano M, Aguilera FS, Osorio E, López-López MT, Cabello I, Toledano-Osorio M, et al. On modeling and nanoanalysis of caries-affected dentin surfaces restored with Zn-containing amalgam and in vitro oral function. Biointerphases 2015;10:041004. https://doi.org/10.1116/1.4933243.

[56] Osorio R, Osorio E, Aguilera FS, Medina-Castillo AL, Toledano M, Toledano-Osorio M. Silver improves collagen structure and stability at demineralized dentin: A dynamic-mechanical and Raman analysis. J Dent 2018;79:61–7. https://doi.org/10.1016/j.jdent.2018.10.003.

[57] Timlin JA, Carden A, Morris MD, Rajachar RM, Kohn DH. Raman Spectroscopic Imaging Markers for Fatigue-Related Microdamage in Bovine Bone. Anal Chem 2000;72:2229–36. https://doi.org/10.1021/ac9913560.

[58] Bertassoni LE, Stankoska K, Swain MV. Insights into the structure and composition of the peritubular dentin organic matrix and the lamina limitans. Micron 2012;43:229–36. https://doi.org/10.1016/j.micron.2011.08.003.

[59] Arabacı T, Kermen E, Özkanlar S, Köse O, Kara A, Kızıldağ A, et al. Therapeutic Effects of Melatonin on Alveolar Bone Resorption After Experimental Periodontitis in

Rats: A Biochemical and Immunohistochemical Study. J Periodontol 2015;86:874–81. https://doi.org/10.1902/jop.2015.140599.

[60] Osorio R, Yamauti M, Osorio E, Ruiz-Requena ME, Pashley DH, Tay FR, et al. Zinc reduces collagen degradation in demineralized human dentin explants. J Dent 2011;39:148–53. https://doi.org/10.1016/j.jdent.2010.11.005.

[61] Posner GH, Switzer Christopher. Total synthesis of natural estrone and estradiol methyl ethers in extremely high enantiomeric purity via an asymmetric Michael addition to an unsaturated sulfoxide. J Am Chem Soc 1986;108:1239–44. https://doi.org/10.1021/ja00266a019.

[62] Price PA, Toroian D, Chan WS. Tissue-nonspecific Alkaline Phosphatase Is Required for the Calcification of Collagen in Serum: a possible mechanism for biomineralization. J Biol Chem 2009;284:4594–604. https://doi.org/10.1074/jbc.M803205200.

[63] Toledano M, Osorio R, Osorio E, Medina-Castillo AL, Toledano-Osorio M, Aguilera FS. Ions-modified nanoparticles affect functional remineralization and energy dissipation through the resin-dentin interface. J Mech Behav Biomed Mater 2017;68:62–79. https://doi.org/10.1016/j.jmbbm.2017.01.026.

[64] Cheng PT, Pritzker KP. Pyrophosphate, phosphate ion interaction: effects on calcium pyrophosphate and calcium hydroxyapatite crystal formation in aqueous solutions. J Rheumatol 1983;10:769–77.

[65] Van Meerbeek B, Vargas M, Inoue S, Yoshida Y, Peumans M, Lambrechts P, et al. Adhesives and cements to promote preservation dentistry. Oper Dent 2001;26:119–44.

[66] Besinis A, van Noort R, Martin N. Remineralization potential of fully demineralized dentin infiltrated with silica and hydroxyapatite nanoparticles. Dent Mater 2014;30:249–62. https://doi.org/10.1016/j.dental.2013.11.014.

[67] Wang C, Wang Y, Huffman NT, Cui C, Yao X, Midura S, et al. Confocal Laser Raman Microspectroscopy of Biomineralization Foci in UMR 106 Osteoblastic Cultures Reveals Temporally Synchronized Protein Changes Preceding and Accompanying Mineral Crystal Deposition. J Biol Chem 2009;284:7100–13. https://doi.org/10.1074/jbc.M805898200.

[68] Awonusi A, Morris MD, Tecklenburg MMJ. Carbonate assignment and calibration in the Raman spectrum of apatite. Calcif Tissue Int 2007;81:46–52. https://doi.org/10.1007/s00223-007-9034-0.

[69] Salehi H, Terrer E, Panayotov I, Levallois B, Jacquot B, Tassery H, et al. Functional mapping of human sound and carious enamel and dentin with Raman spectroscopy. J Biophotonics 2013;6:765–74. https://doi.org/10.1002/jbio.201200095.

[70] Toledano M, Osorio R, Osorio E, García-Godoy F, Toledano-Osorio M, Aguilera FS. Advanced zinc-doped adhesives for high performance at the resin-carious dentin interface. J Mech Behav Biomed Mater 2016;62:247–67. https://doi.org/10.1016/j.jmbbm.2016.05.013.

[71] Farahani RM, Nguyen K-A, Simonian M, Hunter N. Adaptive calcified matrix response of dental pulp to bacterial invasion is associated with establishment of a network of glial fibrillary acidic protein+/glutamine synthetase+ cells. Am J Pathol 2010;177:1901–14. https://doi.org/10.2353/ajpath.2010.100073.

[72] Kinney JH, Marshall GW, Marshall SJ. Three-dimensional mapping of mineral densities in carious dentin: theory and method. Scanning Microsc 1994;8:197–204; discussion 204-205.

Figure and table captions

Fig. 1. Microleakage values (mean and SD) obtained for each experimental group. Identical lower case letter indicate no significant differences between time points at each study group. Same numbers indicate no significant differences among groups within the same time point ($p<0.05$).

Fig. 2. Young's modulus (**a**), tan delta (δ) (**b**) and nanoroughness (**c**) (mean and SD) attained at the different experimental groups. Abbreviations: NPs: nanoparticles; ML-NPs; Melatonine doped nanoparticles. Young's modulus, Tan delta and nanoroughness were analyzed separately.

For each variable: Identical lowercase means no significant difference among distinct NPs at the same dentin half (cervical and apical) at 24 h. Identical capital letter indicates no significant difference between different NPs at the same dentin half (cervical and apical) at 6 m. Identical number indicates no significant difference between different storage time (24 h *vs* 6 m) within the same NPs at the same dentin half (cervical and apical). Asterisks indicate significant difference between different dentin halves (cervical *vs* apical) within the same NPs at the same storage time (24 h and 6 m).

Fig. 3. (**a, d**), 2 x 2 μm topographic mapping obtained by AFM at the inner zone of the cervical (**a**) and apical (**d**) control dentin, after 6 m of storage. Peritubular (PD) and intertubular (ID) dentin structures are evidenced, denoting heterogeneous and rough surfaces. The entrances of dentinal tubules are exposed (asterisks). Multiple microporosities are observed (arrows). (**b, e**), 2 x 2 μm topographic mapping obtained by AFM at the inner zone of the cervical (**b**) and apical (**e**) apical dentin treated with undoped NPs, after 6 m of storage. Irregular and rough surface characterized the dentin view. Tubules were completely (arrow), partially (pointer) occluded or empty (arrowheads). The collagen fibers and the staggered pattern of collagen fibrils are shown (faced arrows).

Remarkable peritubular dentin (PD) was evident. Stick-slip images in radial direction of nucleated minerals resulted observable at the intertubular dentin, as sight of energy dissipation (double pointers). Microcraking of the dentinal tubules wall characterized some empty tubules (double arrows). Demineralized collagen fibers crossed over the intertubular dentin and penetrated the tubular lumen, integrating the tubular wall (asterisk). (**c, f**), 2 x 2 μm topographic mapping obtained by AFM at the inner zone of the cervical (**c**) and apical (**f**) cervical dentin treated with ML-NPs, after 6 m of storage. A smoother dentin surface was shown. Peritubular dentin appeared strongly remineralized (arrows). Evident processes of intertubular and intratubular mineralization, with protruding rounded forms were also observed (asterisks). Some bridge and rod-like new mineral formations were perceived surrounding the intratubular crystals (arrowheads). These crystals precipitated beams held the intratubular deposits of mineral to the peritubular dentin.

Fig. 4. 2D micro-Raman map of the phosphate peak (961 cm^{-1}) intensities at the control group (**a** and **d**), at samples treated with undoped-NPs (**b** and **e**), and ML-NPs (**c** and **f**) at the cervical and apical radicular dentin, respectively, after 6 m of storage.

Fig. 5: Representative FESEM topographic images at the inner zone of the cervical dentin treated with ML-NPs. (**a, b)**, At 24 h time point, peritubular (PD) and intertubular (ID) dentin appeared clearly mineralized. Mineral deposition is completely covering the dentin surface (asterisks). Dentinal tubules were totally filled of mineralized collagen fibrils and NPs (single arrows). Nucleated crystals coating the collagen fibrils and permitting the observation of the D-periodicity banding (67 nm) were detected (double arrows). (**c, d),** At 24 h time point, dentin tubules appeared completely (pointer) or partially (faced arrows) filled, and ID dentin was entirely remineralized. Reduced areas of mineralization were also evident (asterisks). NPs remained totally adhered to the remineralized tubule

wall and collagen fibers in d (arrow heads). (**e, f),** After 6 m of storage, coralline sub-micron formations were observed occupying the dentin surface (pointers), reproducing a net-shaped precipitated crystals and covering both ID and PD (asterisks). The mineral formations did not allow any display of the entrance of tubules and they exhibited multiple amorphous clumps of material scattered and grouped as dense network of buttons-like materials (pointers). A minimal amount of tubules appeared mineral free with a clear ring of peritubular dentin (arrows). Cordon-like crystals formed the surface of intertubular dentin marking the subjacent path of the mineralized collagen fibers (arrow heads).

Table 1. Raman intensities and ratios of mineral and organics components attained from dentin at the different experimental groups.

Figure 1

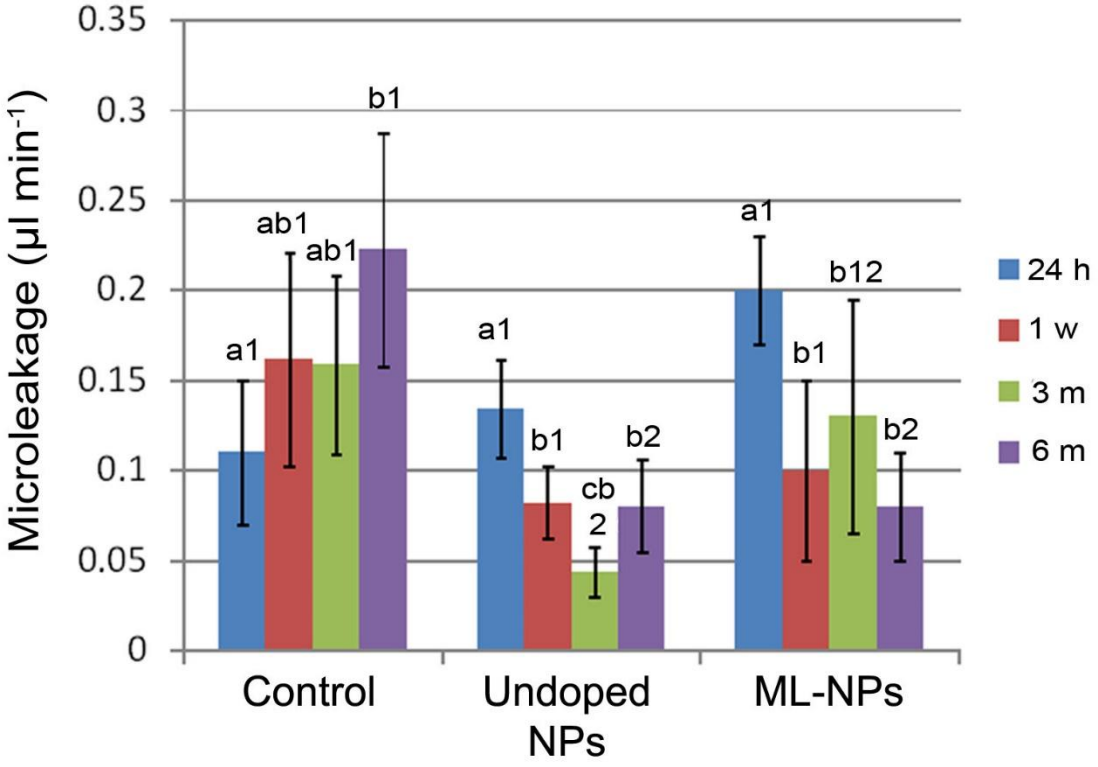
0.35
0.3
0.25
0.2
0.15
0.1
0.05
0
Microleakage (µl min-1)
a1
ab1
ab1
b1
a1
b1
cb
2
b2
a1
b1
b12
b2
Control
Undoped NPs
ML-NPs
24 h
1 w
3 m
6 m

Figure 2

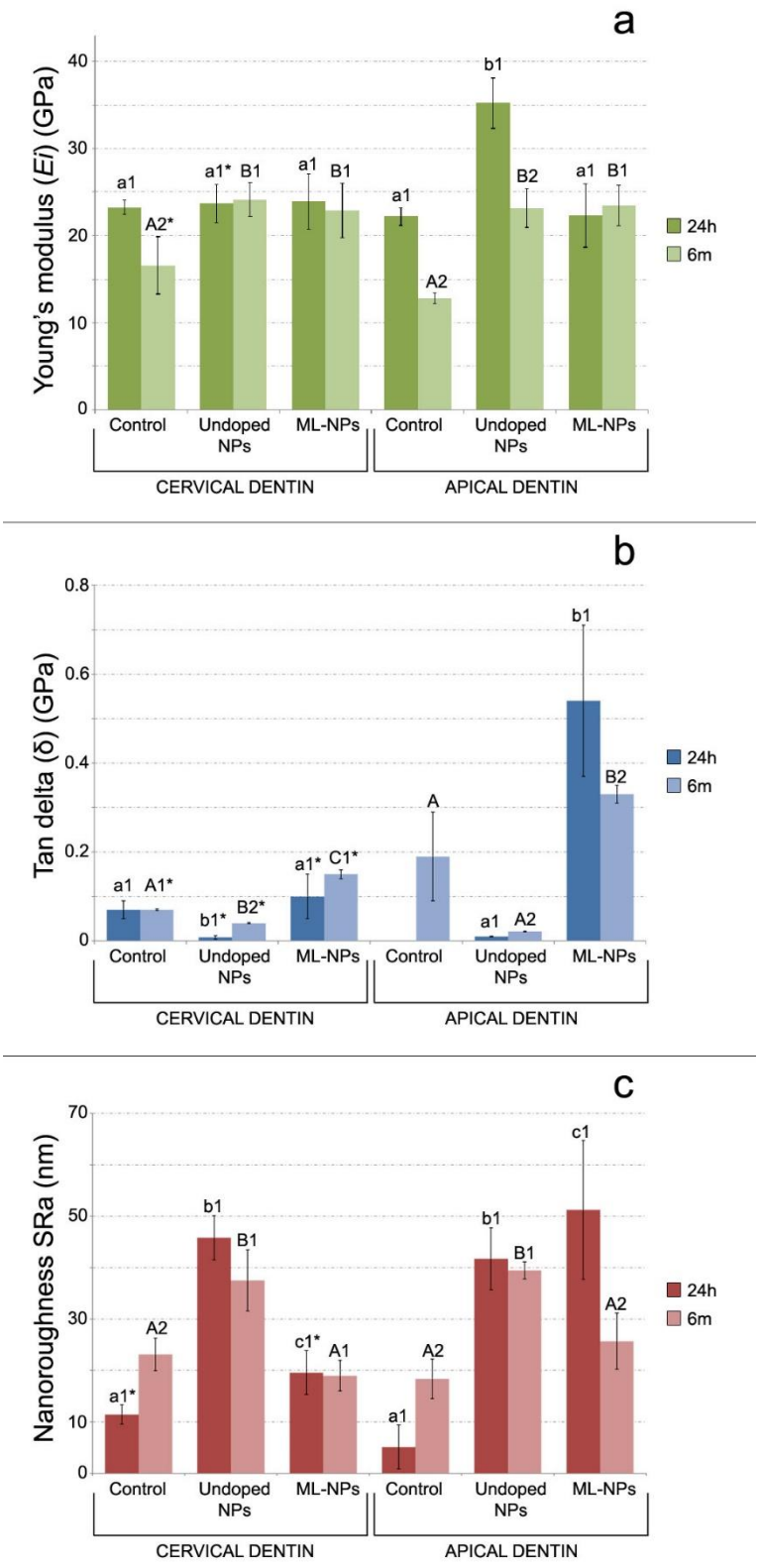
a
Young's modulus (Ei) (GPa)
40
30
20
10
0
a1
A2*
a1* B1
a1 B1
a1
A2
b1
B2
a1 B1
24h
6m
Control
Undoped NPs
ML-NPs
Control
Undoped NPs
ML-NPs
CERVICAL DENTIN
APICAL DENTIN
b
Tan delta (δ) (GPa)
0.8
0.6
0.4
0.2
0
a1 A1*
b1* B2*
a1* C1*
A
a1 A2
b1
B2
24h
6m
Control
Undoped NPs
ML-NPs
Control
Undoped NPs
ML-NPs
CERVICAL DENTIN
APICAL DENTIN
c
Nanoroughness SRa (nm)
70
50
30
10
0
a1*
A2
b1
B1
c1*
A1
a1
A2
b1
B1
c1
A2
24h
6m
Control
Undoped NPs
ML-NPs
Control
Undoped NPs
ML-NPs
CERVICAL DENTIN
APICAL DENTIN

Figure 3

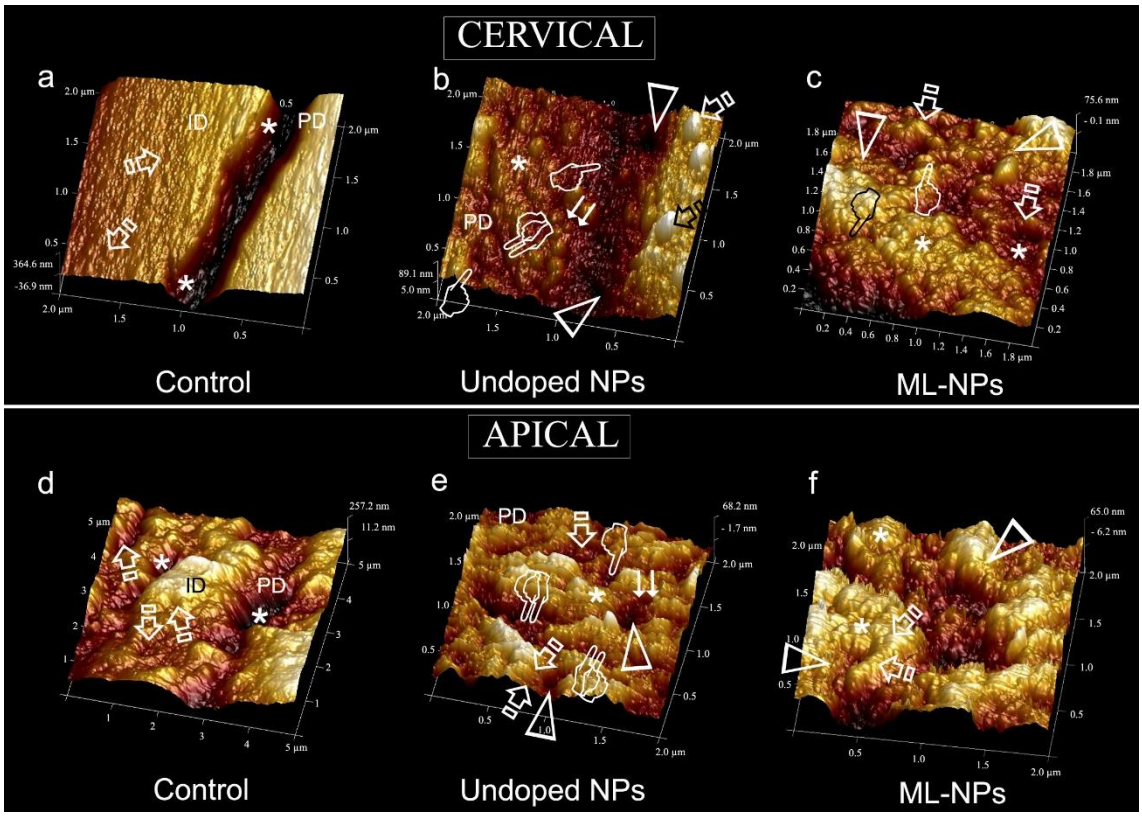

Figure 4

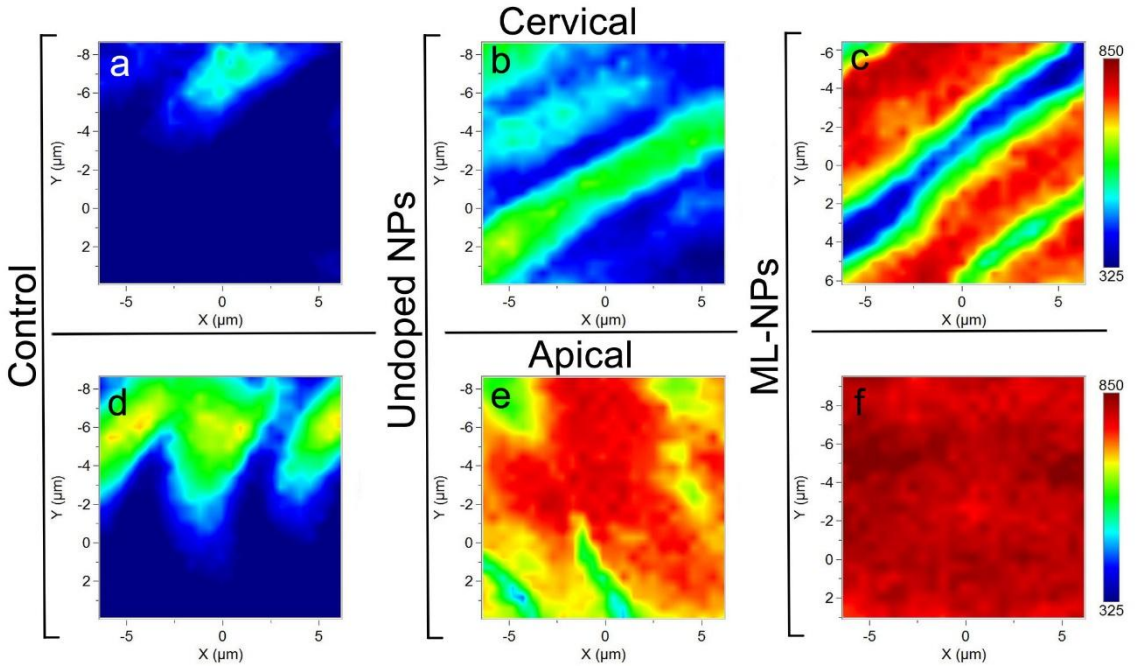

Figure 5

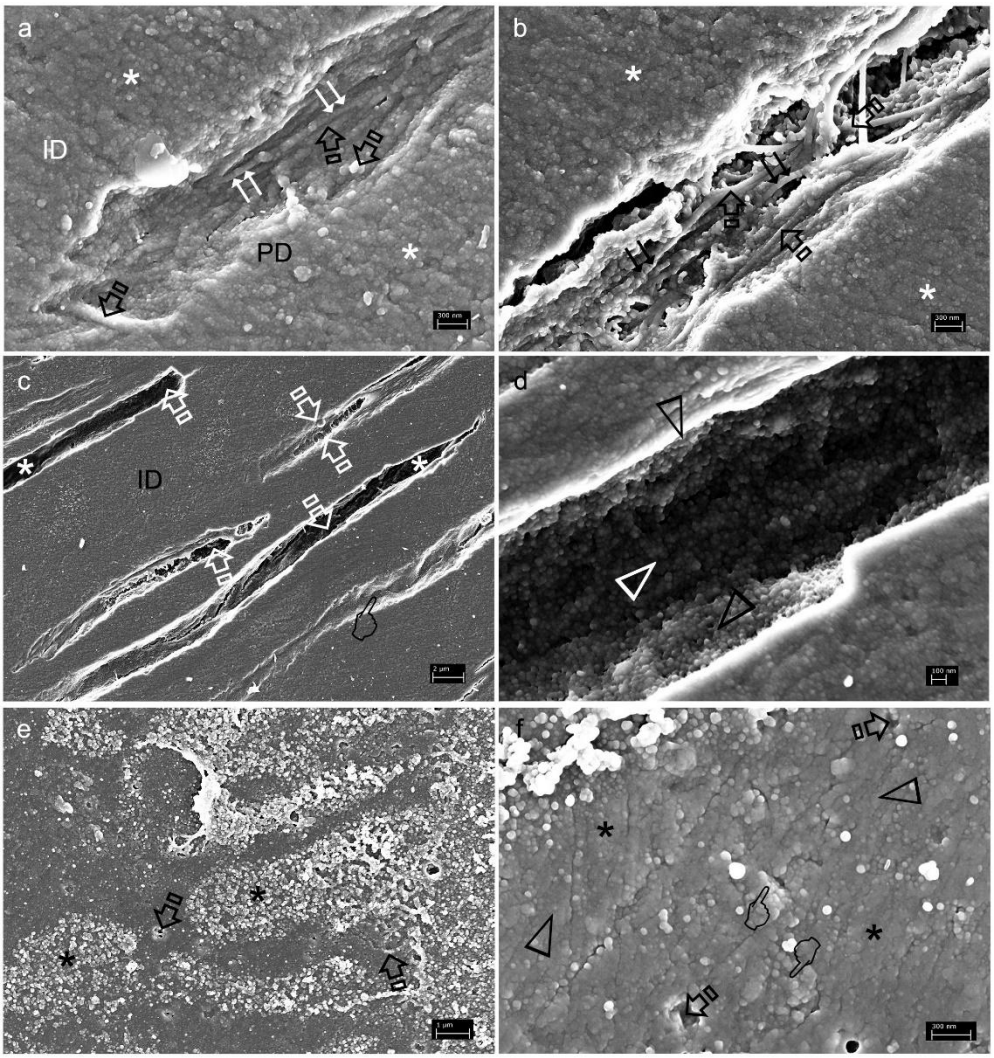

Table 1.

		MINERALS											
		Relative Presence of Mineral											
		Phosphate [960 cm^{-1}]						Stoichiometric HAp [963 cm^{-1}]		Carbonate [1070 cm^{-1}]		Crystallinity [Ratio 1020/ 1030 cm^{-1}]	
		Peak		Area		RMC [960/1003]							
		24h	**6m**	**24h**	**6m**	**24h**	**6m**	**24h**	**6m**	**24h**	**6m**	**24h**	**6m**
Control	Cervical	503.35	347.65	14879	9013	16.20	25.43	391.16	290.92	74.78	38.15	9.46	0.48
	Apical	783.85	581.69	19917	15082	22.43	13.03	619.08	468.67	122.26	66.93	14.25	0.69
Undoped-NPs	Cervical	440.35	528.65	13017	13707	12.82	17.14	351.95	449.06	56.33	64.98	12.75	0.76
	Apical	763.45	733.88	18984	18225	22.01	34.21	632.41	588.79	103.67	99.49	14.76	0.67
ML-NPs	Cervical	725.31	729.6	18429	18135	25.72	21.39	622.82	535.40	96.36	94.9	16.77	0.75
	Apical	711.33	813.11	18043	20210	33.58	31.41	609.21	666.64	110.79	105.3	17.13	0.73

		ORGANICS											
		Crosslinking		Nature of collagen									
		Pyridinium [1032 cm^{-1}]		C-C Hydroxyproline [871 cm^{-1}]		C-C Hydroxilated proline [920 cm^{-1}]		Collagen [937 cm^{-1}]		Lipids and proteins CH_2 [1448 cm^{-1}]		Proteoglycans [1062 cm^{-1}]	
		24h	**6m**	**24h**	**6m**	**24h**	**6m**	**24h**	**6m**	**24h**	**6m**	**24h**	**6m**
Control	Cervical	35.26	17.41	8.32	9.50	37.88	22.14	101.23	66.15	22.96	14.57	63.02	31.54
	Apical	31.27	30.67	15.13	16.37	52.63	28.35	138.89	100.04	25.40	21.71	93.20	55.79
Undoped-NPs	Cervical	26.92	31.63	11.82	14.95	23.39	24.14	75.79	92.1	20.35	22.58	48.00	55.25
	Apical	41.98	34.72	15.26	23.21	33.84	31.17	110.47	102.43	26.20	35.43	83.88	80.07
ML-NPs	Cervical	38.15	46.25	17.64	25.25	33.51	42.46	113.23	117.29	25.93	34.16	83.77	82.61
	Apical	37.06	45.02	30.18	25.44	37.10	40.93	100.74	113.09	40.67	35.84	93.25	92.71

Abbreviations: NPs: Nanoparticles; ML-NPs: Melatonine Nanoparticles; RMC: Relative mineral concentration between mineral/Phenyl (1003); HAp: Hydroxyapatite. For all the components, the peaks values had been normalized to the intensity of the Amide II band basis near 1510 cm^{-1}. Peaks positions are expressed in cm^{-1}.

Supporting Information

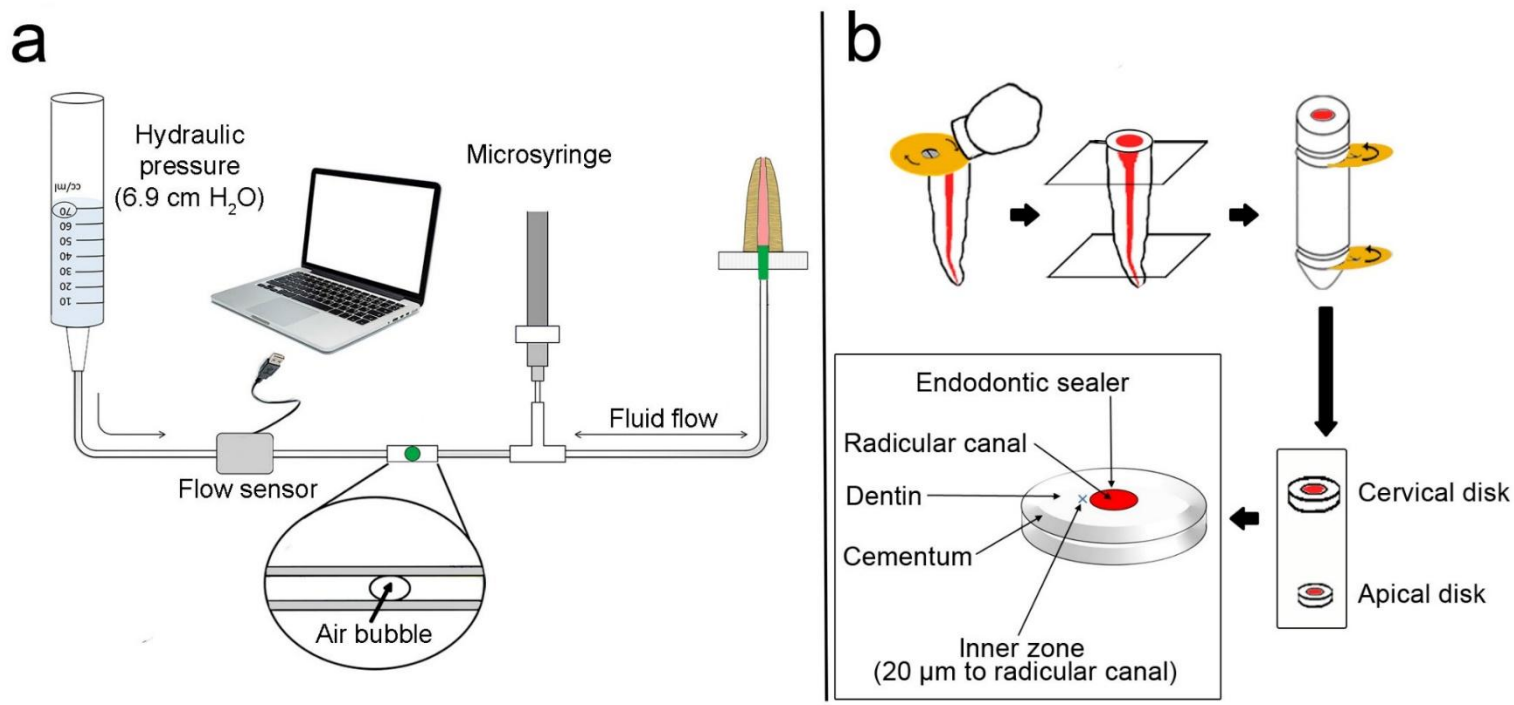

Fig. S1 (a), Schematic illustration showing how dentin permeability was assessed. Samples were connected to a hydraulic pressure device under a constant hydraulic pressure. The dimensions of the changes in fluid volume were attained via a digital sensor. (**b)**, Schematic representation of the specimen preparation for interfacial assessment. Tooth coronal section was eliminated. Two disks of cervical and apical root dentin were obtained. Inner dentin zones were measured.

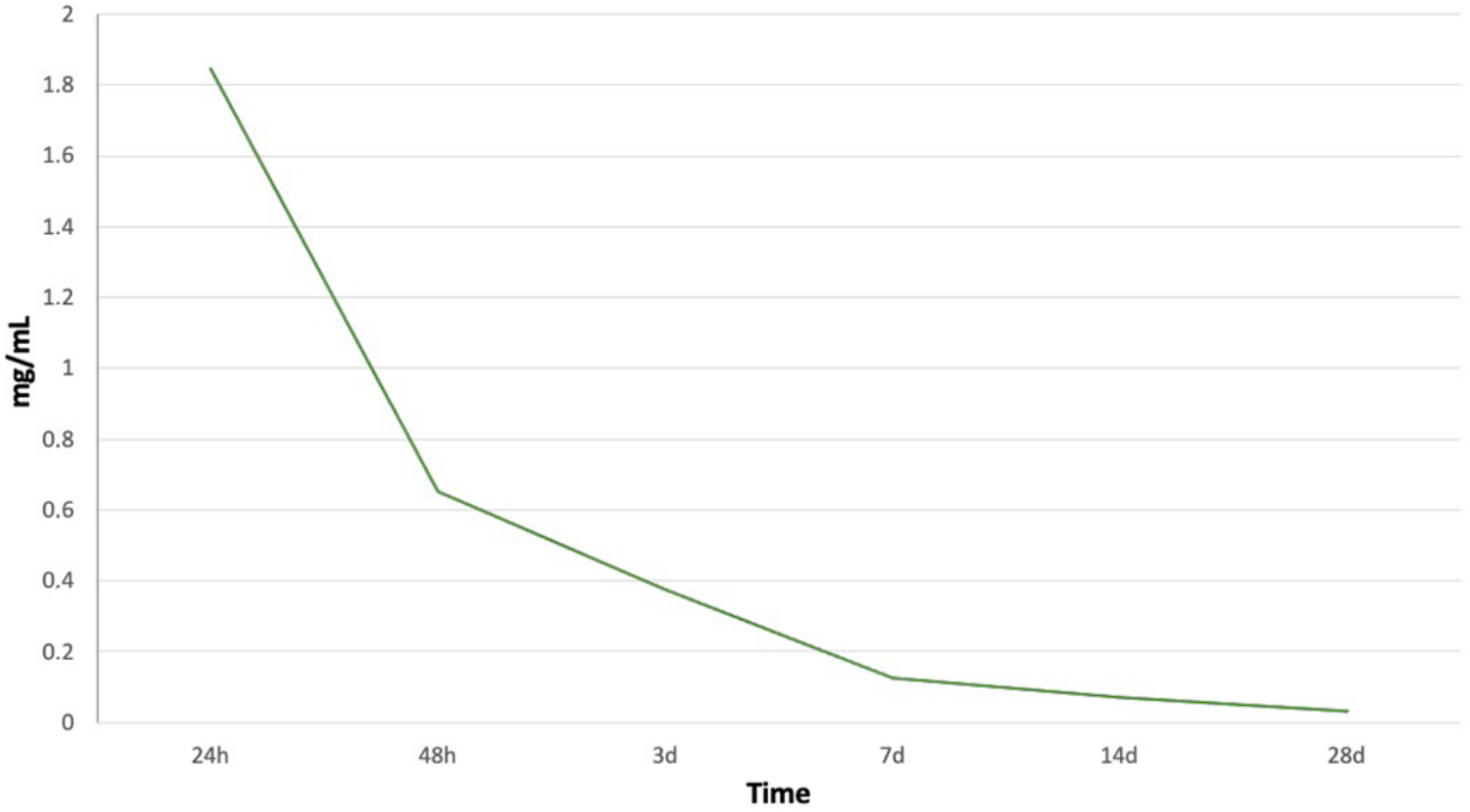

Fig. S2. Melatonin liberation profile curve. Mean values are expressed in mg/mL released per 10 mg of NPs, at each time point.

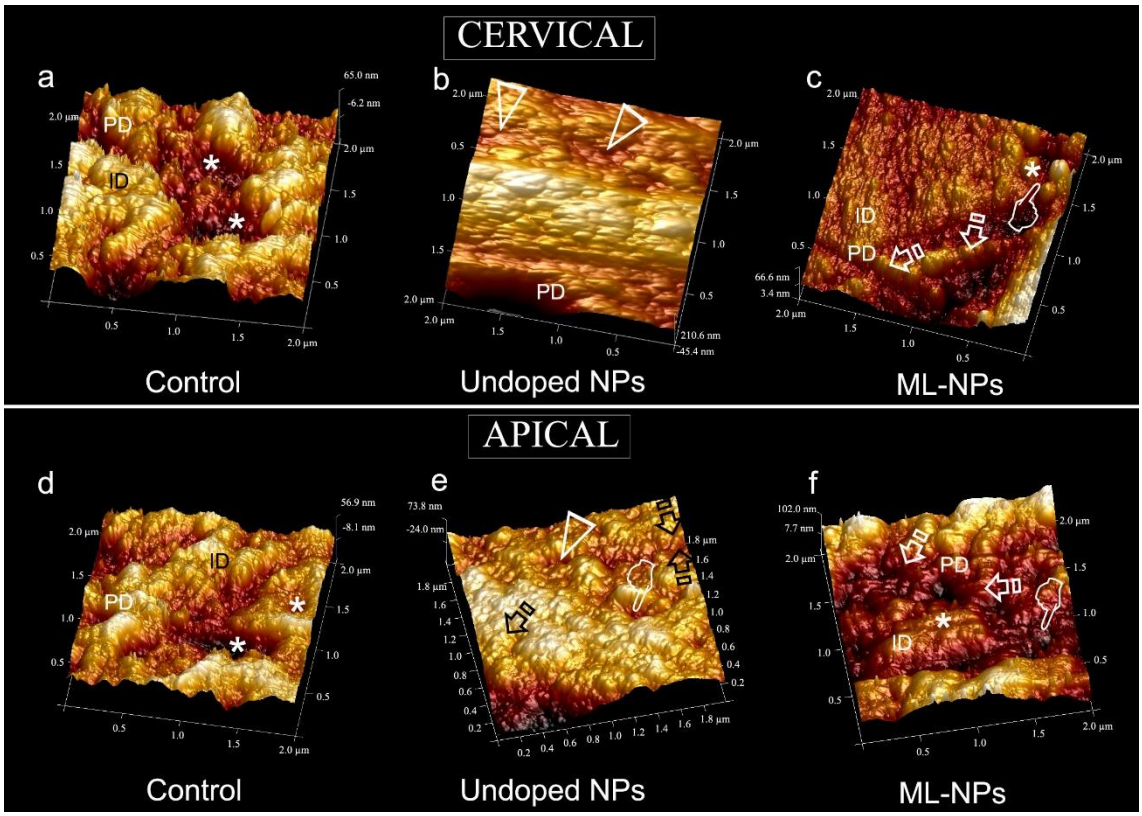

Fig. S3. (**a, d**), 2 x 2 µm topographic mapping obtained by AFM at the inner zone of the apical dentin at control specimens, after 24 h of storage. Peritubular (PD) and intertubular (ID) dentin structures are shown. Some entrances of dentinal tubules are observed (asterisks). (**b, e**), 2 x 2 µm topographic mapping obtained by AFM at the inner zone of the apical dentin treated with undoped-NPs, after 24 h of storage. Irregular and rough surface characterized the dentin view. Tubules were completely (arrow), partially (pointer) occluded or empty (arrowheads). The collagen fibers and the staggered pattern of collagen fibrils are shown (faced arrows). (**c, f**), 2 x 2 µm topographic mapping obtained by AFM at cervical dentin treated with ML-NPs, after 24 h of storage. Peritubular dentin is deeply remineralized (arrows). Intertubular and intratubular mineralization, were also evidenced (asterisks). Crystals precipitated beams linked the intratubular mineral deposits to the peritubular dentin.

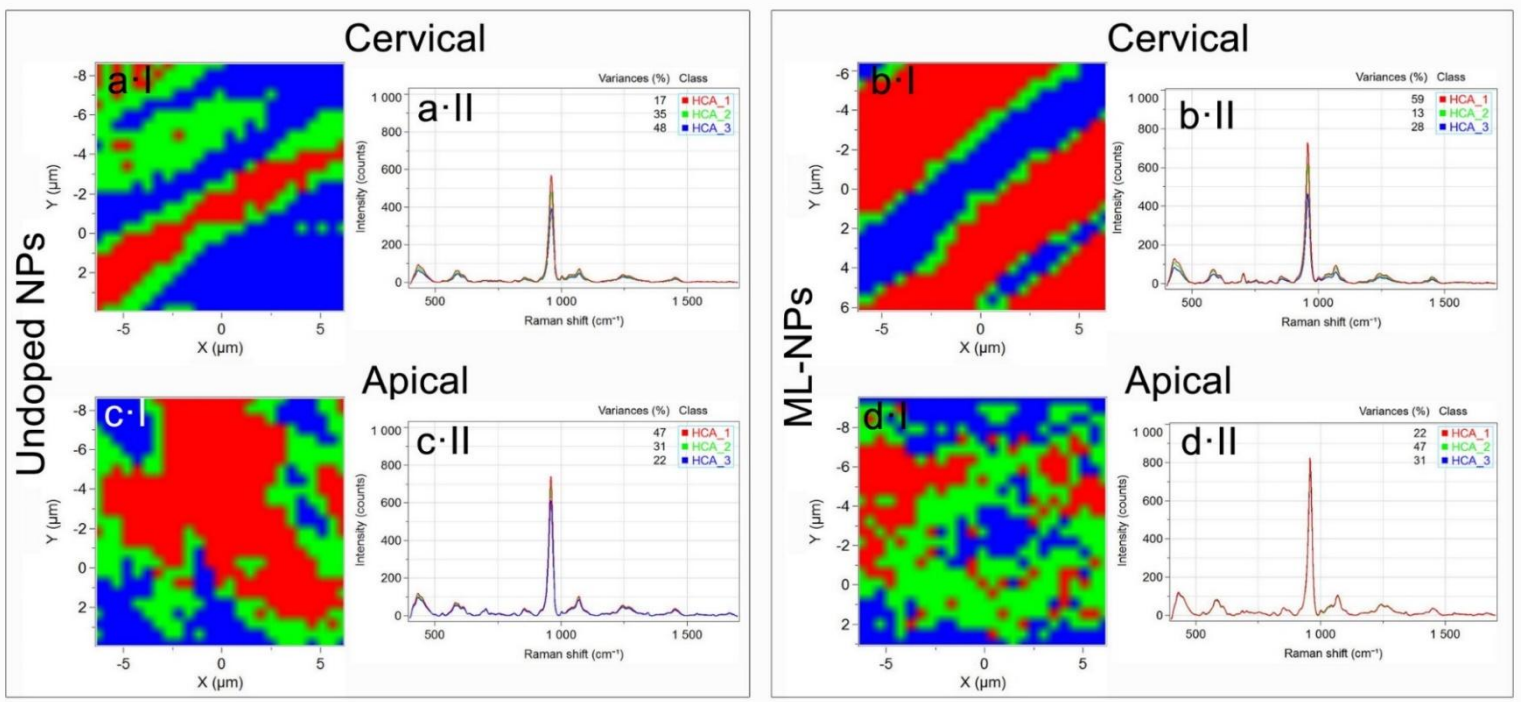

Fig S4. Colour mapping from hierarchical cluster analysis **(**HCA) images and results corresponding to dentin treated with undoped-NPs (a, c) and M-NPs (b, d) at the cervical and apical radicular dentin, respectively, after 6 m of storage. Three levels of HCA clustering are shown. Areas of distinct colour have differences in Raman spectral distribution and chemical composition. Each cluster, corresponding to a different dentin remineralization stage, is assigned to a different colour (red, green, and blue), hence obtaining a false colour-image of the substrate on the basis of similar spectral features.

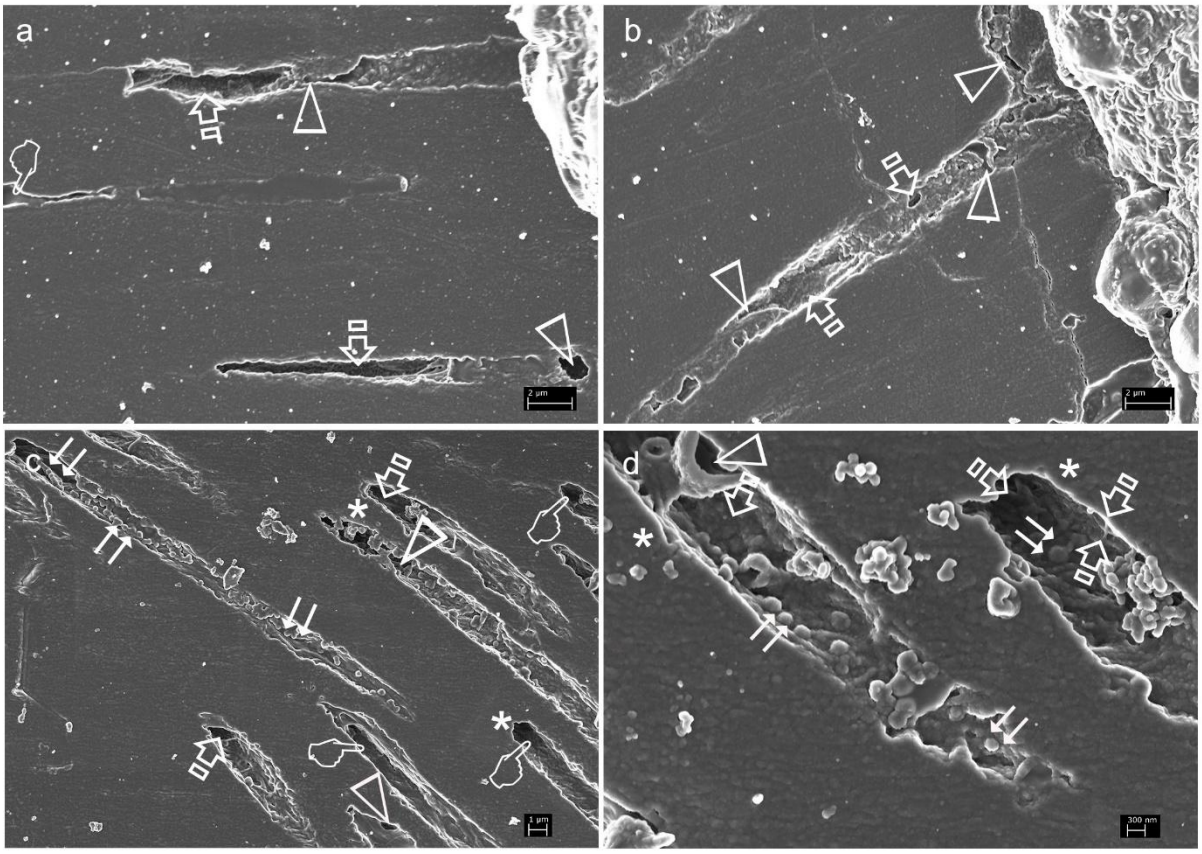

Fig S5. Representative FESEM topographic images at the inner zone of the apical dentin of control specimens, after 6 m of storage (**a, b**).The resin-dentin interface shows a lack of adaptation between both substrates unveiling multiple gaps (arrowheads). Gaps were also showed at the canal sealer and dentin interface when specimens were treated with undoped-NPs (**c, d**) at cervical halves of root dentin after 6 m time point. Dentinal tubules were partially mineral filled, allowing multiple empty spaces (single arrows). Some tubules appeared mineral free (pointers) but with a robust peritubular dentin wall (asterisks). NPs were clearly observed filling the dentinal tubules (doubled arrows), and intimately close to the collagen fibers, some of which appeared demineralized (faced arrows).

Table 1.

		MINERALS											
		Relative Presence of Mineral											
		Phosphate [960 cm^{-1}]						Stoichiometric HAp [963 cm^{-1}]		Carbonate [1070 cm^{-1}]		Crystallinity [Ratio 1020/ 1030 cm^{-1}]	
		Peak		Area		RMC [960/1003]							
		24h	**6m**	**24h**	**6m**	**24h**	**6m**	**24h**	**6m**	**24h**	**6m**	**24h**	**6m**
Control	Cervical	503.35	347.65	14879	9013	16.20	25.43	391.16	290.92	74.78	38.15	9.46	0.48
	Apical	783.85	581.69	19917	15082	22.43	13.03	619.08	468.67	122.26	66.93	14.25	0.69
Undoped-NPs	Cervical	440.35	528.65	13017	13707	12.82	17.14	351.95	449.06	56.33	64.98	12.75	0.76
	Apical	763.45	733.88	18984	18225	22.01	34.21	632.41	588.79	103.67	99.49	14.76	0.67
ML-NPs	Cervical	725.31	729.6	18429	18135	25.72	21.39	622.82	535.40	96.36	94.9	16.77	0.75
	Apical	711.33	813.11	18043	20210	33.58	31.41	609.21	666.64	110.79	105.3	17.13	0.73

		ORGANICS											
		Crosslinking		Nature of collagen									
		Pyridinium [1032 cm^{-1}]		C-C Hydroxyproline [871 cm^{-1}]		C-C Hydroxilated proline [920 cm^{-1}]		Collagen [937 cm^{-1}]		Lipids and proteins CH_2 [1448 cm^{-1}]		Proteoglycans [1062 cm^{-1}]	
		24h	**6m**	**24h**	**6m**	**24h**	**6m**	**24h**	**6m**	**24h**	**6m**	**24h**	**6m**
Control	Cervical	35.26	17.41	8.32	9.50	37.88	22.14	101.23	66.15	22.96	14.57	63.02	31.54
	Apical	31.27	30.67	15.13	16.37	52.63	28.35	138.89	100.04	25.40	21.71	93.20	55.79
Undoped-NPs	Cervical	26.92	31.63	11.82	14.95	23.39	24.14	75.79	92.1	20.35	22.58	48.00	55.25
	Apical	41.98	34.72	15.26	23.21	33.84	31.17	110.47	102.43	26.20	35.43	83.88	80.07
ML-NPs	Cervical	38.15	46.25	17.64	25.25	33.51	42.46	113.23	117.29	25.93	34.16	83.77	82.61
	Apical	37.06	45.02	30.18	25.44	37.10	40.93	100.74	113.09	40.67	35.84	93.25	92.71

Abbreviations: NPs: Nanoparticles; ML-NPs: Melatonine Nanoparticles; RMC: Relative mineral concentration between mineral/Phenyl (1003); HAp: Hydroxyapatite. For all the components, the peaks values had been normalized to the intensity of the Amide II band basis near 1510 cm^{-1}. Peaks positions are expressed in cm^{-1}.